buildings

Article

Monitoring of Wind Effects on a Super-Tall Building under a Typhoon

Haoran Pan, **Jiurong Wu** and **Jiyang Fu** *

Research Center for Wind Engineering and Engineering Vibration, Guangzhou University, Guangzhou 510006, China
* Correspondence: jiyangfu@gzhu.edu.cn

Abstract: Field measurements are critical to further understand the structural behavior of super-tall buildings under strong wind actions. This paper presents field measurements that reflect the wind characteristics and wind effects on Leatop Plaza under Typhoon Vicente. Wind field characteristics, including the turbulence intensity, gust factor, and power spectral density of wind speed in an urban area, were obtained on the basis of a statistical analysis of measured wind data. Subsequently, measured wind-induced accelerations were used to evaluate the dynamic characteristics of the building and the effects of wind on it. On the basis of the first several modes, the modal properties, i.e., the natural frequency and damping ratio, were identified via the fast Bayesian fast Fourier transform method and compared with those identified using the stochastic subspace method. The discrepancy between the identified results and finite element model predictions is presented and discussed. Finally, the variation in the modal parameters with respect to time and the vibration amplitude was analyzed while considering the associated posterior uncertainty.

Keywords: wind effect; field measurement; super-tall building; damping; modal identification

check for updates

Citation: Pan, H.; Wu, J.; Fu, J. Monitoring of Wind Effects on a Super-Tall Building under a Typhoon. *Buildings* **2023**, *13*, 47. https://doi.org/10.3390/buildings13010047

Academic Editors: Husam Hussein, Yanping Zhu and Rafea F. Hassan

Received: 21 November 2022
Revised: 13 December 2022
Accepted: 20 December 2022
Published: 25 December 2022

1. Introduction

The development of economic construction and advancements in construction technology have resulted in a significant increase in the number of super-tall buildings worldwide. Generally, super-tall buildings are more flexible and more lightly damped than mid- or low-rise buildings, and their wind-induced response under strong winds is the most important factor that determines their safety and comfort. Field measurements allow one to directly understand the dynamic structural characteristics (i.e., the natural frequency, damping ratio, and mode shape) of prototype buildings; in fact, they provide useful information for finite element model (FEM) updating, damage detection, structural performance monitoring, etc. In recent decades, numerous field measurement studies pertaining to tall/super-tall buildings have been conducted [1–5]. Ohkuma [1] conducted field measurements of a 68 m steel structure to measure its along-wind and cross-wind accelerations in strong winds and identified its frequencies and damping characteristics. Kijewski-Correa et al. [4] performed a long-term real-time monitoring of multiple super-tall buildings in Chicago, USA, to identify their modal parameters as well as to verify wind tunnel test results and basic assumptions introduced in an FEM. Fu et al. [5] conducted a field study to investigate the wind characteristics, wind-induced responses, and wind-induced pressure of the Guangzhou West Tower (450 m) in Guangzhou, China, and compared the field-measured results with wind tunnel test predictions.

Modal parameters determine the accuracy of estimated wind-induced responses of super-tall buildings [6]. Therefore, modal parameter variations in field studies, particularly damping, are of interest to the structural-wind community and have received significant attention in recent decades. However, the damping ratios identified from field data often indicate large dispersion owing to various factors, such as the foundation type, geological condition, structural material, and nodal connection form. Jeary [7–9] investigated the nonlinear characteristics of structural damping ratios on the basis of field measurements and proposed a trilinear damping model. Tamura and Suganuma [10] employed the random decrement technique (RDT) to assess the structural dynamic properties of three high-rise towers under strong winds and discovered that the damping ratio increased with the amplitude of the structure, whereas the frequency decreased as the amplitude increased. Li et al. [11–13] conducted numerous field measurements on super-tall buildings in several coastal cities in China, such as Hong Kong, Shenzhen, and Shanghai, and confirmed the nonlinear dependence of damping on amplitude. Meanwhile, a few studies indicate the insignificant correlation between damping and amplitude based on field measurements [14–17], whereas the time-varying trend of damping has been reported [18,19].

The Leatop Plaza is a 303 m high super-tall building situated in Guangzhou, China. Guangzhou is a coastal city that is affected by typhoons during the summer. Thus, a wind and structural monitoring system, which included anemometers on the roof and accelerometers at multiple heights, was established to provide in situ measurement information regarding the wind field and structural responses. Field measurements at multiple heights of a high-rise building under typhoons are rarely investigated, owing to budget, accessibility, and technical issues such as synchronization. On the basis of multilevel records, the mode shape of the abovementioned building can be obtained, which is beneficial for the subsequent updating of the FEM.

This paper presents the wind characteristics measured at 303 m above ground and the structural responses of the Leatop Plaza during Typhoon Vicente. The fast Bayesian fast Fourier transform (FFT) method was utilized for modal identification, and the identified modal parameters were compared with those identified via stochastic subspace identification (SSI) and the prediction results of the FEM. A detailed analysis of the variation in the modal parameters is presented in addition to the associated posterior uncertainty considered. Notably, a field measurement on the Canton Tower (461 m), which is approximately 2 km south of Leatop Plaza, was also conducted under the same typhoon event, and the modal parameters were identified using the RDT in a previous study [20]. However, the RDT can yield misleading results when the signal is contaminated by noise [21], and it does not reveal the uncertainty of the identified results. However, the fast Bayesian FFT approach adopted in this study can provide the most plausible value of the modal parameter and its associated uncertainty. Consequently, the systematic trends can be ascertained on the basis of the identification inaccuracies arising from modeling errors and measurement noise.

The remainder of this paper is organized as follows: The monitoring system of the building and the typhoon event are described in Section 2, followed by the measured wind characteristics in Section 3. In Section 4, the results of the structural response, modal identification via the fast Bayesian FFT and SSI methods, comparison with the FEM prediction, and variations of the modal parameters are presented and discussed. The main results and conclusions are presented in Section 5.

2. Field Monitoring Program

2.1. Building Instrumentation

Leatop Plaza (Figure 1) is located in the central business district (CBD) of Guangzhou (Figure 2), China; it comprises 65 floors above ground, its cross-section measures 45.7 m $\times$ 45.7 m, and its height is 303 m. Its structure is primarily composed of a reinforced concrete tube and an external steel frame, and there are no additional dampers on the building. A monitoring system was installed at the Leatop Plaza to monitor the wind-induced response and the wind characteristics around the building. Four bi-axial low-frequency accelerometers were installed orthogonally along the two main axes ("x": east–west and "y": north–south) of the building on the 38th, 44th, 52nd, and 58th floors. All accelerometers were placed at the centroid of the building's cross-section. Meanwhile, a three-dimensional (3D) ultrasonic anemometer was installed approximately 3 m atop the building, where the wind azimuth angle γ is 0° when the wind blows from the north (see Figure 2), and the elevation angle is defined as positive when the winds blow from below.

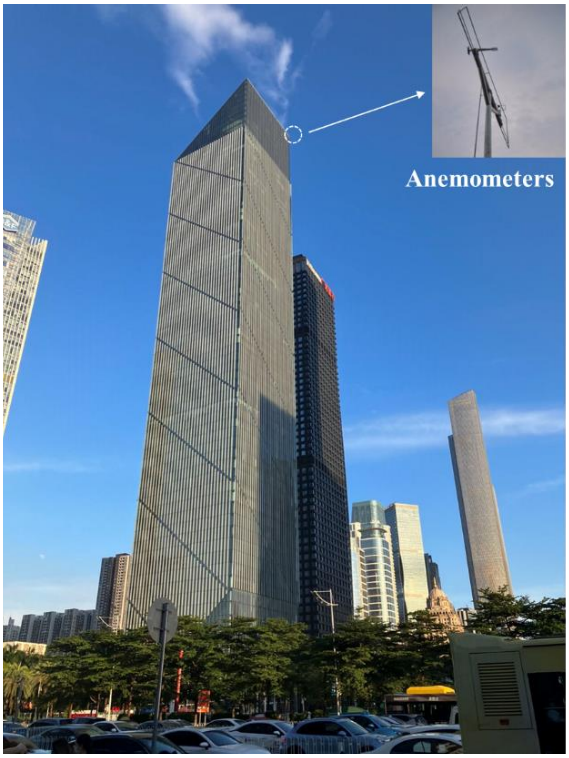

Figure 1. Overview of Leatop Plaza.

Figure 2. Measurement site location.

2.2. Typhoon Vicente

Typhoon Vicente is one of the strongest tropical cyclones experienced in the Chinese province of Guangdong in recent decades. It formed as a tropical depression on 20 July 2012, northeast of Manila, the Philippines, and soon propagated west–northwest. Vicente intensified rapidly to a severe typhoon over the South China Sea and propagated toward the region west of the Pearl River Estuary. It resulted in landfall near the coastal area of Taishan in Guangdong, China, which is approximately 100 km from Guangzhou, before dawn on 24 July 2012, and subsequently weakened into a typhoon. Figure 3 shows the path of Typhoon Vicente.

Figure 3. Path of Typhoon Vicente.

3. Wind Characteristics

3.1. Mean Wind Speed and Direction

The time histories of the wind speed $u(i)$, azimuth angle $\gamma(i)$, and elevation angle $\beta(i)$ measured using a 3D ultrasonic anemometer are shown in Figure 4. To obtain the mean wind speeds and directions, the wind speed was decomposed into orthogonal x- and y-directions as follows:

$$\begin{aligned} u_x(i) &= u(i)\cos\beta(i)\cos\gamma(i) \\ u_y(i) &= u(i)\cos\beta(i)\sin\gamma(i) \end{aligned} \tag{1}$$

Subsequently, the horizontal mean wind speed U and mean wind direction α can be determined as follows:

$$\begin{aligned} \overline{u_x} &= \frac{1}{N}\sum_{i=1}^{N} u_x(i) \\ \overline{u_y} &= \frac{1}{N}\sum_{i=1}^{N} u_y(i) \\ U &= \sqrt{\overline{u_x}^2 + \overline{u_y}^2} \\ \alpha &= \arcsin\left(\frac{\overline{u_x}}{U}\right) + H[-\overline{u_y}] \times 180^{\circ} \end{aligned} \tag{2}$$

where $H[.]$ is the Heaviside (or unit) step function. Next, the fluctuating longitudinal and lateral components of wind speed can be calculated as follows:

$$\begin{aligned} \widetilde{u}(i) &= u_x(i)\cos\alpha + u_y(i)\sin\alpha - U \\ \widetilde{v}(i) &= -u_x(i)\sin\alpha + u_y(i)\cos\alpha \end{aligned} \tag{3}$$

The time histories of the 3 min mean wind speed (scaler), wind direction, and wind speed in the vertical direction (scaler) are displayed in Figure 5. As shown in Figure 5a,c, the mean wind speed varied from 7 to 13 m/s, and the mean wind speed in the vertical direction was 3.5–7 m/s, which suggests a large vertical component of the mean wind speed. This is attributable to the leading edge of the roof when the wind blows from the east, as the mean wind direction varied between 70° and 110° (Figure 5b). However, the mean wind speed was much lower than around 20 m/s measured at a height of 461 m at the Canton Tower [20] within the same period. This was primarily due to the discrepancy in wind fields over different heights and locations. Specifically, Leatop Plaza is located in the CBD of the city and is surrounded by many tall buildings, whereas Canton Tower is located in a more open area and is much taller than its surrounding buildings. Thus, the wind flows of the latter are less affected by the urban canopy, which is consistent with the observations in a previous study [22].

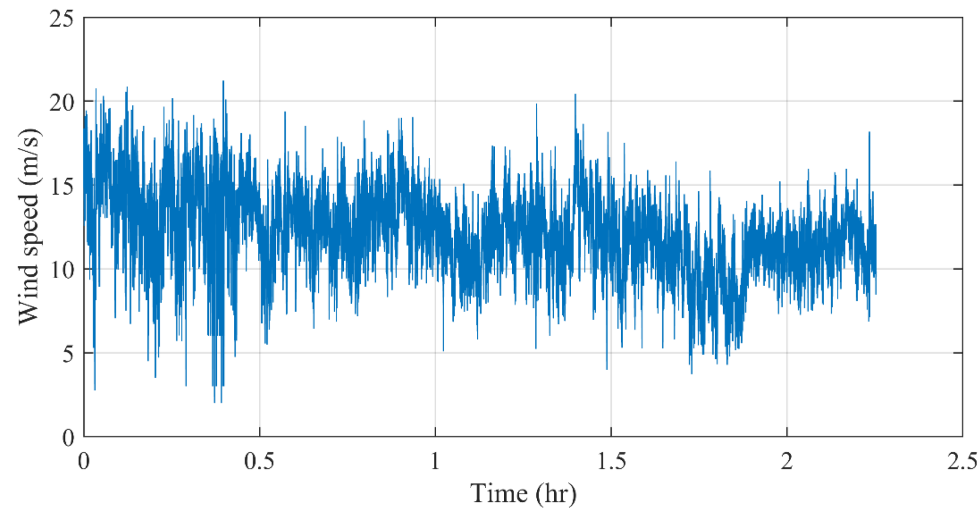

(**a**)

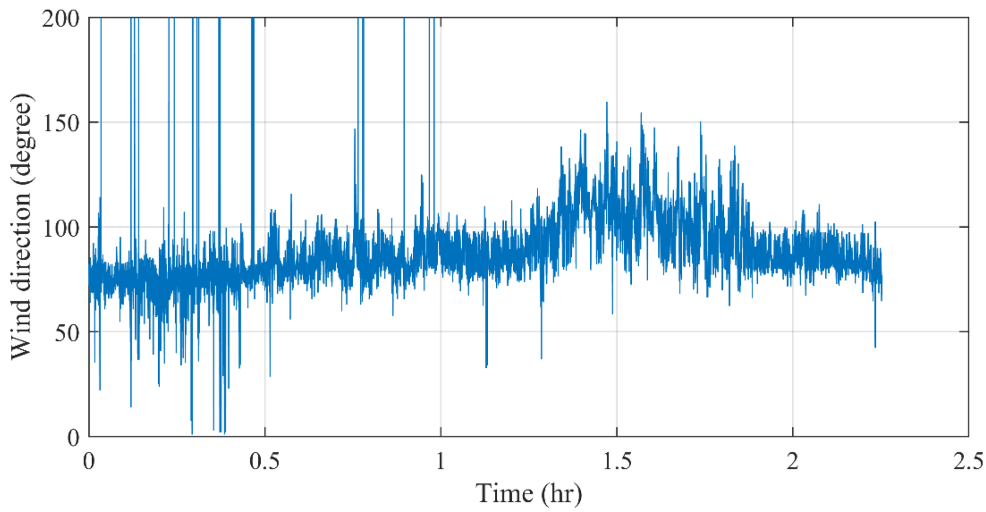

(**b**)

Figure 4. *Cont.*

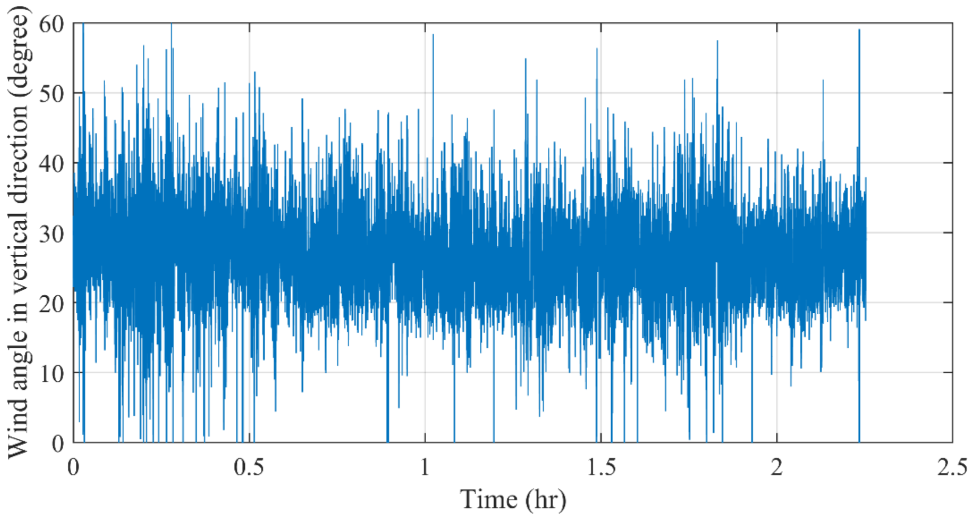

(**c**)

Figure 4. Time histories of wind speed, wind direction, and wind angle in vertical direction measured using ultrasonic anemometer (origin: 12:13 July 24): (**a**) wind speed; (**b**) wind direction; (**c**) wind angle in the vertical direction.

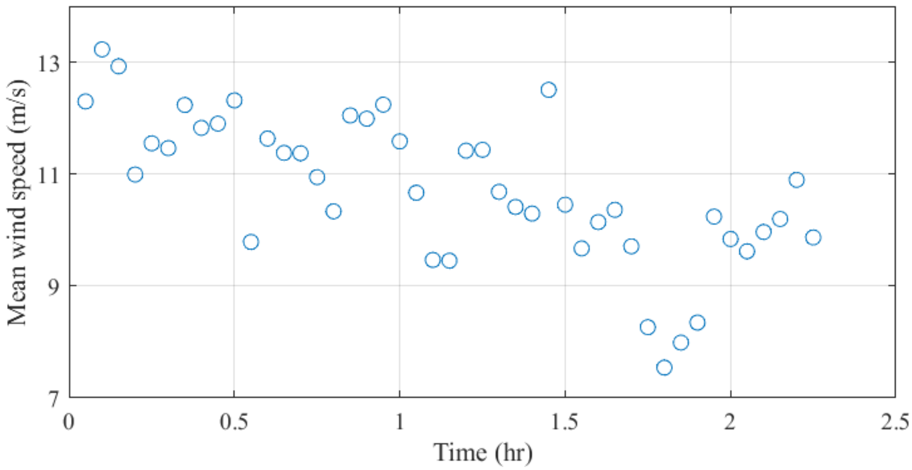

(**a**)

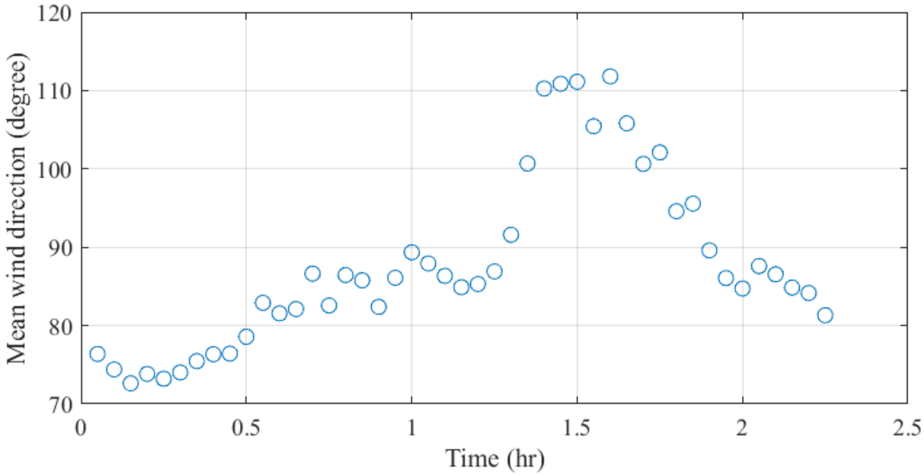

(**b**)

Figure 5. *Cont.*

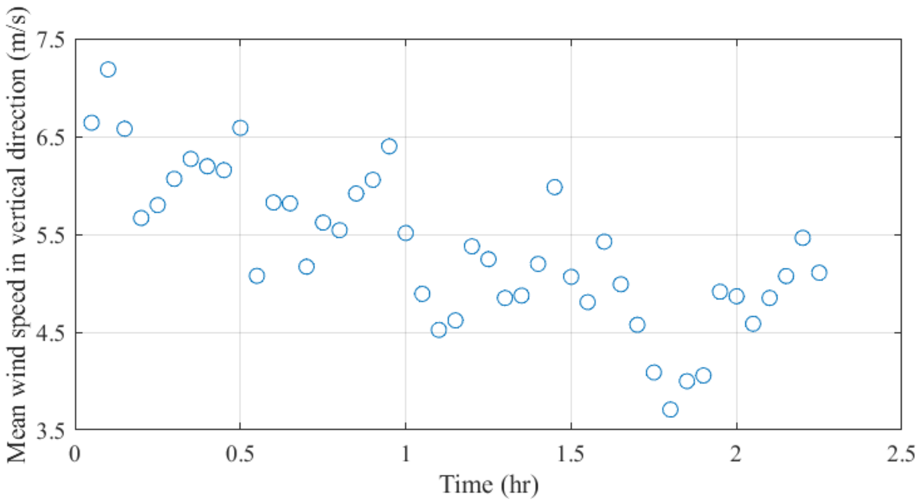

(**c**)

Figure 5. Variations in mean wind speed, mean wind direction, and mean wind speed in vertical direction: (**a**) mean wind speed; (**b**) mean wind direction; (**c**) mean wind speed in the vertical direction.

3.2. Turbulence Intensity, Gust Factor, and Power Spectral Density (PSD)

The turbulence intensity in the longitudinal and lateral directions is expressed as follows:

$$I_u = \frac{\sigma_i}{U}(i = u, v) \tag{4}$$

where σ_i $(i = u, v)$ is the standard deviation of the fluctuating wind-speed components in the longitudinal (u) and lateral directions (v).

Figure 6 shows the variations in the turbulence intensity based on a 3 min mean wind speed in the longitudinal and lateral directions. In general, the turbulence intensity in both directions decreased when the mean wind speed increased. The average values of the turbulence intensity in the longitudinal and lateral directions were 0.15 and 0.13, respectively, and the ratio between them was $\sigma_u : \sigma_v = 1 : 0.90$. According to Chinese design code GB 50009-2012 [23], the longitudinal turbulence intensity can be estimated using the empirical equation $I_u(z) = I_{10}(\frac{z}{10})^{-\alpha}$. On the basis of the deployment height of the anemometer $z = 306$ m, nominal turbulence intensity $I_{10} = 0.39$, and exponent $\alpha = 0.3$ (the terrain type of Leatop Plaza is type D), the longitudinal turbulence intensity was estimated to be 0.14, which was similar to the measured value of 0.15.

The gust factor is defined as the ratio of the gust speed within the gust duration t_g (typically 3 s) to the mean wind speed.

$$\begin{aligned} G_u(t_g) &= 1 + \frac{\max(\overline{u(t_g)})}{U} \\ G_v(t_g) &= \frac{\max(\overline{v(t_g)})}{U} \end{aligned} \tag{5}$$

Figure 7 shows the relationship between the gust factor and turbulence intensity in the longitudinal direction, i.e., the gust factor increased gradually with the turbulence intensity. As indicated in previous studies [24,25], the relationship between the longitudinal gust factor and longitudinal turbulence intensity can be fitted using the following empirical equation:

$$G_u(t_g) = 1 + k_1 {I_u}^{k_2}(T/t_g) \tag{6}$$

where T is the time duration for the mean wind speed, k_1 and k_2 are the regression parameters, and t_g is the gust duration. By fitting the empirical equation to the field measurement data, k_1 and k_2 were estimated to be 0.34 and 0.94, respectively.

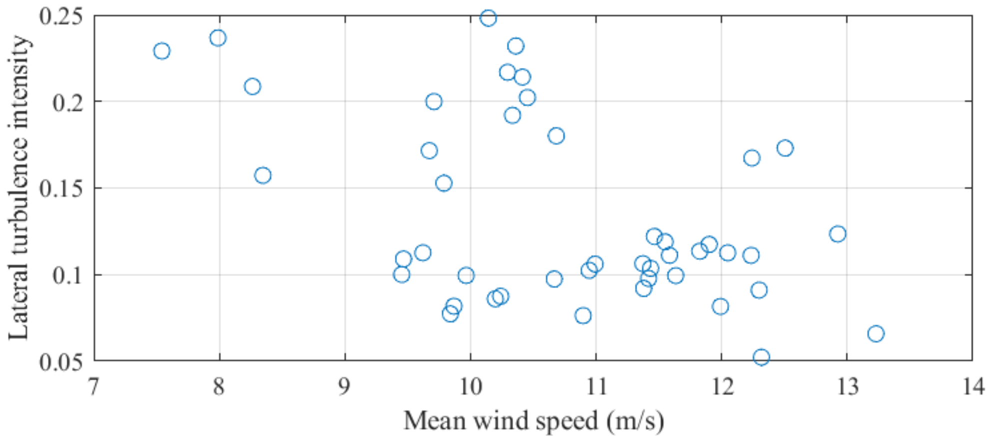

(**a**)

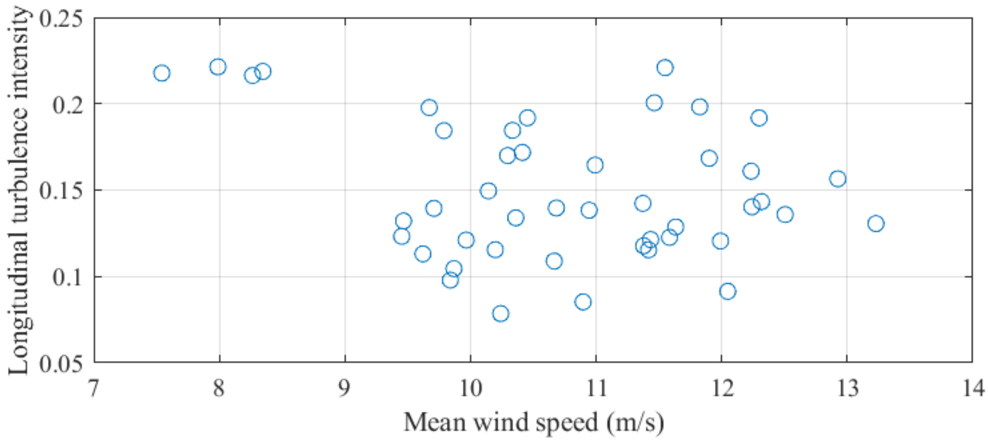

(**b**)

Figure 6. Relationship between turbulence intensity and mean wind speed: (**a**) longitudinal direction; (**b**) lateral direction.

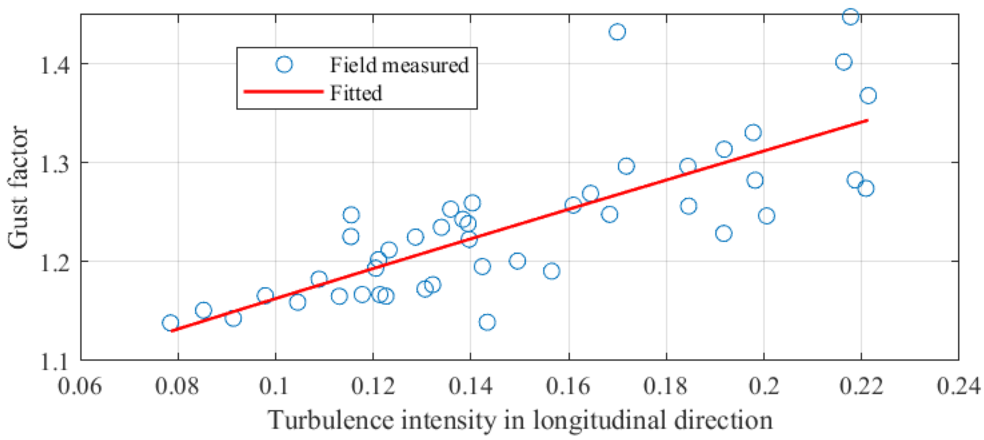

Figure 7. Relationship between gust factor and longitudinal turbulence intensity.

Among several spectra, the von Karman spectrum has been widely recognized as a suitable representation of wind speed spectra for expressing the energy distribution of fluctuating wind speeds, whose normalized spectral expressions are as follows:

$$\begin{aligned} \frac{fS_u(f)}{\sigma_u^2} &= \frac{4L_u f/U}{\left[1+70.8(L_u f/U)^2\right]^{5/6}} \\ \frac{fS_v(f)}{\sigma_v^2} &= \frac{4L_v f/U\left[1+755.2(L_v f/U)^2\right]}{\left[1+283.2(L_u f/U)^2\right]^{11/6}} \end{aligned} \tag{7}$$

Here, f is the frequency; σ_u^2 and σ_v^2 are the variances of the fluctuating wind speed in the longitudinal and lateral directions, respectively; L_u and L_v are the estimated turbulence integral length scales in the longitudinal and lateral directions, respectively; and $S_u(f)$ and $S_v(f)$ are the PSDs of fluctuating wind speed in the longitudinal and lateral directions, respectively. The turbulence integral length scale is expressed as follows:

$$L_i = \frac{U}{\sigma_i^2} \times \int_0^{\infty} R_i(\tau)\mathrm{d}\tau,\ (i = u, v) \tag{8}$$

where $R_i(\tau)$ is the auto-covariance function of the wind speed fluctuation. In applications, the turbulence integral length scale can be readily determined by fitting the wind speed spectrum, for example, by fitting Equation (7) using the von Karman spectrum.

The normalized PSDs of the fluctuating wind speed in the longitudinal and lateral directions obtained using field data involving a relatively high wind speed and steady wind direction are shown in Figure 8. For comparison, the von Karman spectrum is superimposed in the figure. The measured spectral density functions of the fluctuating wind speed in the longitudinal and lateral directions were consistent with the von Karman spectrum in the lower frequency range ($f/U < 10^{-3}$), whereas a slight difference was observed in the higher frequency range. This suggests that the von Karman spectrum is suitable for describing the energy distribution of fluctuating wind speeds at approximately 300 m above the central district of Guangzhou.

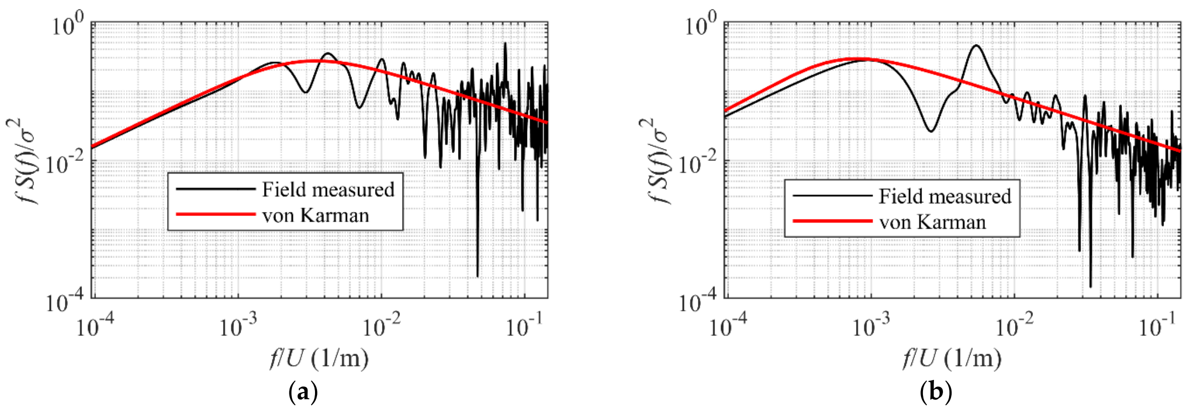

Figure 8. Power spectral density of fluctuating wind speed: (**a**) longitudinal direction; (**b**) lateral direction.

4. Structural Performance and Dynamic Properties

4.1. Structural Acceleration Response

Figure 9 shows the time history of the measured accelerations on the 38th, 44th, 52nd, and 58th floors. The peak values on the 58th floor were 2 and 3 milli-g in the x- and y-directions, respectively. The measured maximum accelerations were significantly less than the occupancy comfort value specified in the local design code [23], i.e., 25 milli-g for office buildings/hotels with a return period of 10 years. This indicates that the wind-induced response of Leatop Plaza provided satisfactory occupant comfort under Typhoon Vicente.

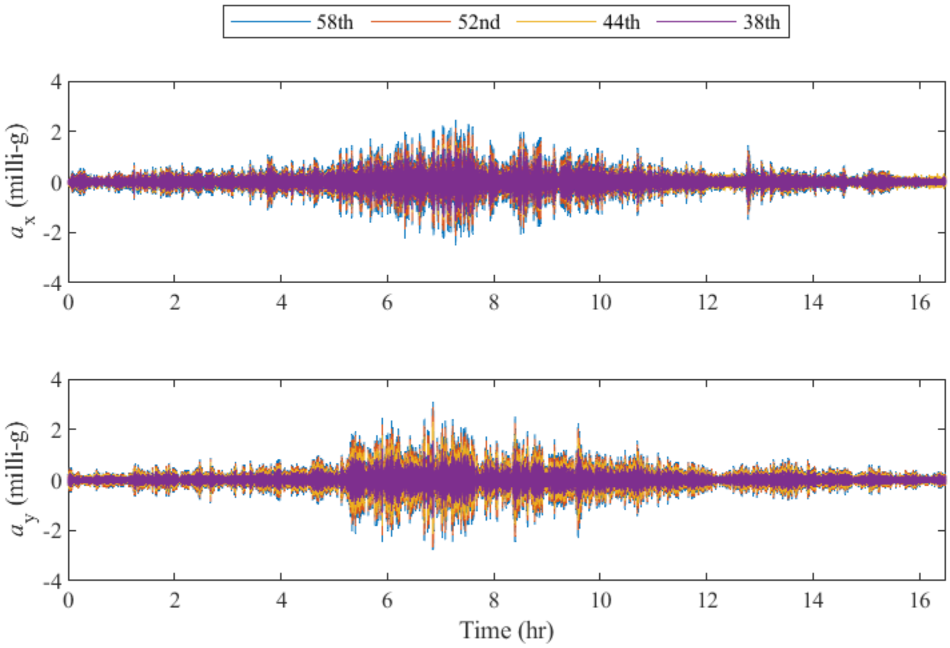

Figure 9. Time history of Leatop Plaza under Typhoon Vicente (origin: 22:30 July 23).

4.2. Structural Dynamic Properties

4.2.1. Method for Modal Analysis

The variations in the modal parameters were investigated on the basis of the results obtained using the fast Bayesian FFT approach, which is a frequency-domain method within the Bayesian operational modal analysis framework [26–28]. The fast Bayesian FFT approach can identify the natural frequency, damping ratio, PSD of the modal force, PSD of the prediction error, and mode shape.

Let vector $\boldsymbol{\theta}$ be the modal parameter to be identified, which can be the natural frequency, damping ratio, PSD of the modal force, PSD of the prediction error, and mode shape, and $\ddot{\boldsymbol{y}}_j$ be the measured acceleration time history of a structure. Therefore, the measured acceleration can be expressed as

$$\ddot{\boldsymbol{y}}_j = \ddot{\boldsymbol{x}}_j(\boldsymbol{\theta}) + \boldsymbol{\varepsilon}_j \; j = 0, 1, 2, \ldots, N-1 \tag{9}$$

where $\ddot{\boldsymbol{x}}_j \in R^n$ is the theoretical acceleration response of the structure, $\boldsymbol{\varepsilon}_j \in R^n$ is the prediction error, N is the number of sampling points, and n is the number of measured degrees of freedom (DOFs).

In this method, the FFT of $\ddot{\boldsymbol{y}}_j$ at frequency $F_k = k/N\Delta t$ is expressed as

$$F_k = \sqrt{\frac{2\Delta t}{N}} \sum_{j=0}^{N-1} \ddot{\boldsymbol{y}}_j e^{-2\pi ijk/N} \tag{10}$$

where $\boldsymbol{i}^2 = -1$, Δt (s) is the sampling interval.

In modal identification, only FFT data within a selected frequency band dominated by the mode(s) of interest are utilized, which is denoted by $\{F_k\}$. According to Bayes' theorem and assuming no prior information, the posterior PDF of $\boldsymbol{\theta}$ can be expressed as

$$p(\boldsymbol{\theta}|\{F_k\}) \propto p(\{F_k\}|\boldsymbol{\theta}) \tag{11}$$

For a large N and small Δt, the FFT at different frequencies can be shown to be asymptotically independent and that their real and imaginary components show a Gaussian distribution. This is mathematically expressed as follows:

$$p(\{F_k\}|\boldsymbol{\theta}) = \prod\nolimits_k \frac{1}{(\pi)^n|\boldsymbol{E}_k|} exp\left[-F_k^* \boldsymbol{E}_k{}^{-1} F_k\right] \tag{12}$$

where |.| is the determinant and $\boldsymbol{E}_k$ denotes the complex-valued, Hermitian covariance matrix of F_k.

$$\boldsymbol{E}_k = \boldsymbol{\Phi}\boldsymbol{H}_k\boldsymbol{\Phi}^T + S_e\boldsymbol{I}_n \tag{13}$$

Here, $\boldsymbol{\Phi} = [\boldsymbol{\varphi}_1, \boldsymbol{\varphi}_2, \ldots, \boldsymbol{\varphi}_m] \in R^{n\times m}$ is the mode shape matrix, with $\boldsymbol{\varphi}_i$ $(i = 1, \ldots, m)$ being the i-th mode shape confined to the measured DOFs only, $\boldsymbol{I}_n \in R^n$ denoting the identity matrix, and $\boldsymbol{H}_k \in R^{m\times m}$ being the transfer matrix whose (i,j) element is expressed as

$$\boldsymbol{H}_k(i,j) = \frac{S_{ij}}{[({\beta_{ik}}^2 - 1) + 2\boldsymbol{i}\zeta_i\beta_{ik}][({\beta_{ik}}^2 - 1) - 2\boldsymbol{i}\zeta_i\beta_{ik}]} \tag{14}$$

Here, $\beta_{ik} = f_i/\mathrm{f}_k$, where f_i is the natural frequency of the i-th mode; $F_k = k/N\Delta t$ is the FFT frequency; and S_{ij} is the cross-spectral density between the i-th and j-th modal excitations (per unit modal mass). To facilitate optimization, the negative log-likelihood function

$$L(\boldsymbol{\theta}) = -\ln p(\{F_k\}|\boldsymbol{\theta}) = nN_f \ln \pi + \sum\nolimits_k \ln \det \boldsymbol{E}_k(\boldsymbol{\theta}) + F_k^* \boldsymbol{E}_k^{-1} F_k \tag{15}$$

is utilized such that

$$p(\boldsymbol{\theta}|\{F_k\}) \propto exp[-L(\boldsymbol{\theta})] \tag{16}$$

Subsequently, the most probable value (MPV) of $\boldsymbol{\theta}$ can be determined by minimizing $L(\boldsymbol{\theta})$. Fast algorithms have been proposed to address the ill-conditioned minimization process and computation issue associated with increasing DOFs. This allows the MPV and covariance matrix to be obtained efficiently in both well-separated modes, or in general [29]. Meanwhile, the uncertainty of identified parameters can be evaluated on the basis of the "coefficient of variation (c.o.v.)", which is defined as the ratio of the posterior standard derivation to the MPV.

4.2.2. Analysis Results

The root PSD and root singular value (SV) spectra of the measured acceleration data under low vibration amplitudes during Vicente based on a 30 min period are presented in Figure 10. Four potential modes were indicated below 1 Hz, and their characteristics were determined on the basis of the identified mode shape. Here, TX1 and TY1 represent the first translational modes along the x- and y-directions, respectively, whereas TX2 and TY2 represent the second translational modes along the x- and y-directions, respectively. As the first two modes were extremely near each other, they were identified simultaneously later on the basis of the assumption that they were located in the 0.15–0.22 Hz band. As for the third and fourth modes, their resonance bands overlapped. Thus, they were identified in the same band, i.e., 0.63–0.80 Hz, assuming two modes.

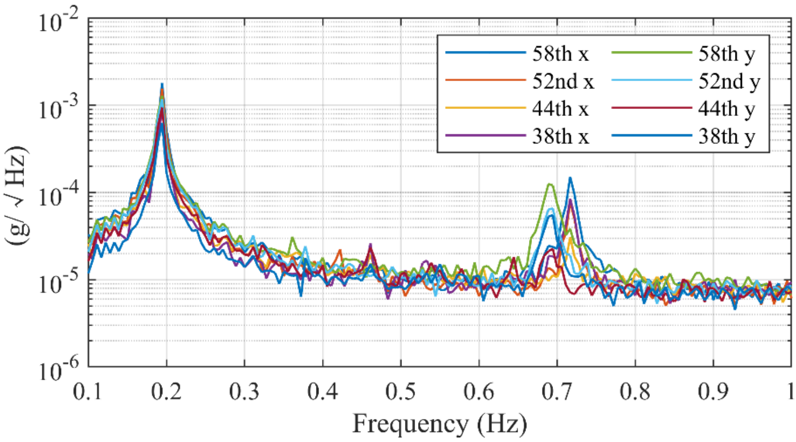

(a)

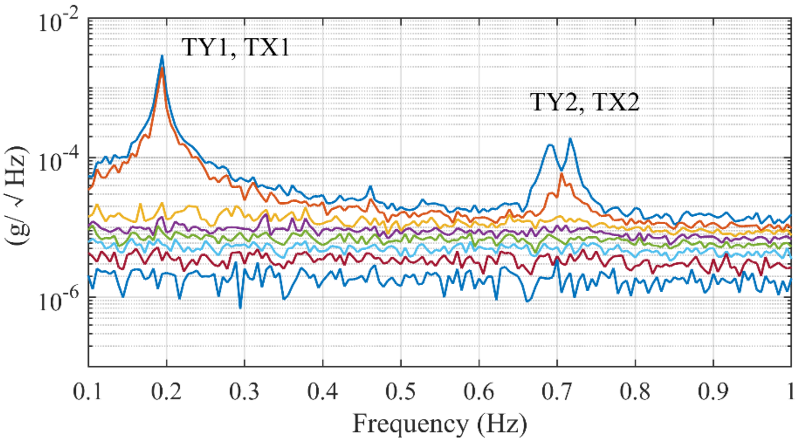

(b)

Figure 10. PSD and SV spectra of a 30 min period: (**a**) PSD; (**b**) SV.

Table 1 shows the modal identification results, including the MPV and posterior c.o.v. of the four modes according to the abovementioned 30 min measured data. The c.o.v.s of the frequencies were less than 0.2%. By contrast, the damping ratios indicate much higher c.o.v.s than the frequencies, i.e., by an order of magnitude. This indicates that the estimation accuracy of the natural frequency is much higher than that of damping, which is consistent with the results of previous studies [14,30]. To verify the accuracy of the Bayesian method, the identification results were obtained using the SSI method [31] on the basis of the measured accelerations (see Table 1). The results show that the frequencies of the different modes were consistent with those obtained using the Bayesian method. However, the damping ratios yielded by both methods were different. This indicates a significant uncertainty in the identified damping ratios, as indicated by their c.o.v.s according to the Bayesian method.

Table 1. Modal parameters identified via the Bayesian approach and SSI.

Mode	Bayesian				SSI	
	f (Hz)	c.o.v. (%)	ζ (%)	c.o.v. (%)	f (Hz)	ζ (%)
TY1	0.187	0.17	0.61	28.6	0.187	0.55
TX1	0.189	0.15	0.49	31.7	0.189	0.37
TY2	0.686	0.09	0.57	16.6	0.686	0.74
TX2	0.712	0.08	0.41	19.1	0.712	0.43

Table 2 presents the frequencies predicted by the FEM in the ETABS software [32], which appear to be lower than the measured values, with a maximum relative difference of 16%. This is attributable to the mass/stiffness difference between the design model and actual building. A more accurate FEM can be obtained by updating the current model on the basis of a comparison of the field-identified modal parameters and their counterparts in the FEM. Notably, the identification results presented herein were only used as reference because the modal parameters may be different during strong winds, as is shown later.

Table 2. Modal parameters predicted by FEM.

Mode	*f* (Hz)	Difference
TY1	0.164	14.0%
TX1	0.167	13.2%
TY2	0.592	15.9%
TX2	0.612	16.3%

Next, the variations in the modal parameters with time was investigated using the Bayesian method. Figures 11 and 12 illustrate the variations in the natural frequencies and damping ratios according to the plus and minus two standard derivations ($\pm 2\sigma$) confidence interval for the four modes during Vicente. As shown in Figure 11, the first two modes, i.e., f_{TY1} and f_{TX1}, began to decrease on the morning of July 24, 2012, as the intensity of the structural response increased; subsequently, they increased as the responses weakened. Similar trends were similarly observed for higher modes f_{TY2} and f_{TX2}. However, all frequencies gradually recovered to their original levels, except for f_{TY2}. The largest reductions of the frequencies for the above-mentioned four modes were 1.87%, 1.56%, 1.84%, and 1.55%. Similarly, Figure 12 shows the time histories of the damping ratios, which included those of both structural and aerodynamic damping. The damping ratios of different modes fluctuated with time but remained in the same order of magnitude. Moreover, no significant time-varying trend was observed. The average values of damping ratios for the four modes were 0.79%, 0.78%, 0.60%, and 0.60%.

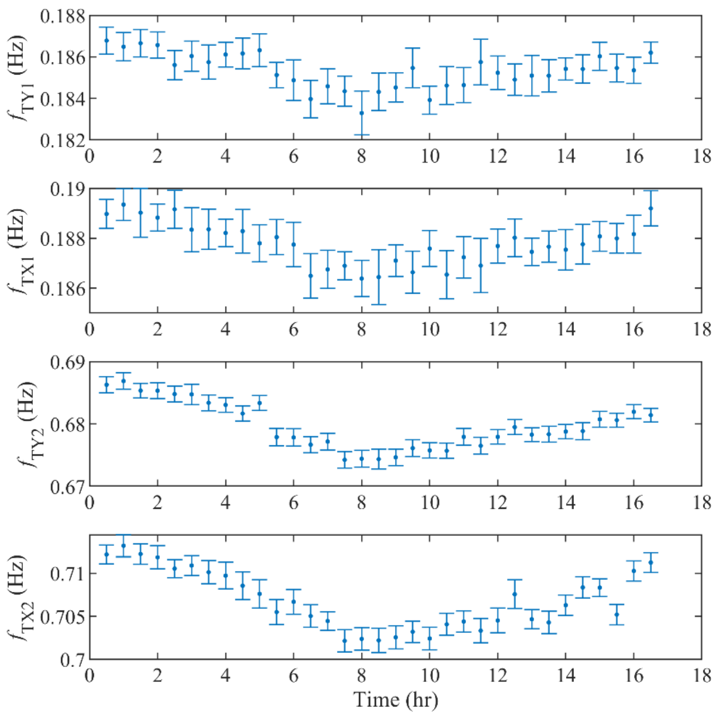

Figure 11. Time history of the identified frequency.

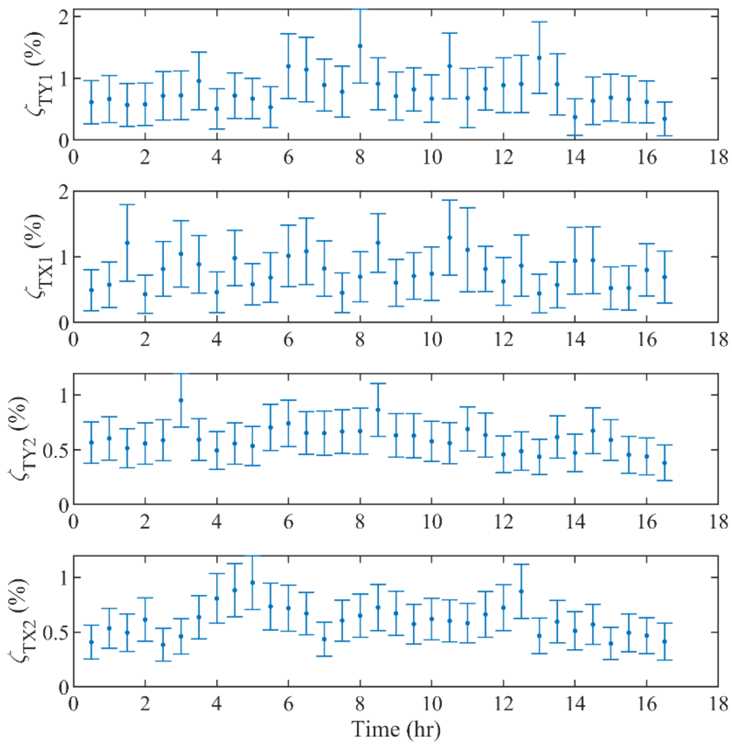

Figure 12. Time history of the identified damping ratio.

Figure 13 shows the identified mode shapes for the four modes. In particular, Figure 13 shows the characteristics of the corresponding mode shapes identified from three periods, namely, the strong-wind period (5:30–6:00, 24 July) and two weak-wind periods (22:30–23:00, 23 July and 14:30–15:00, 24 July) indicated in the work of Hua et al. [20]. As is shown, the mode shapes remained unchanged during the typhoon.

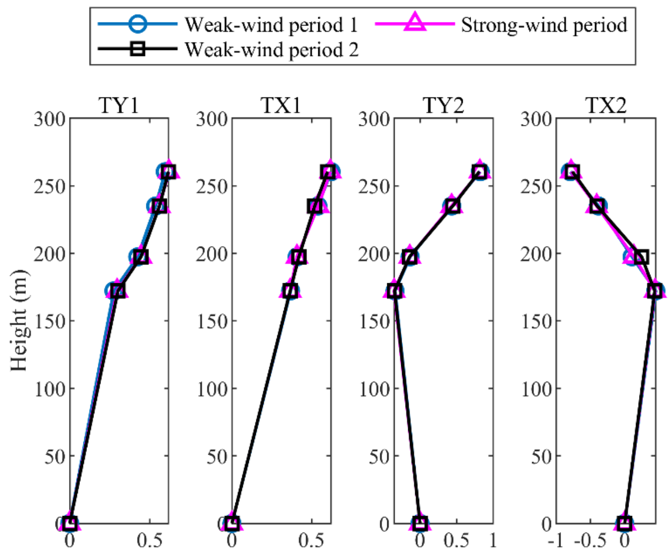

Figure 13. Variation in mode shape.

Finally, we investigated the possible correlation between the identified natural frequency and damping ratio with the modal acceleration root mean square (RMS) for a specified mode [30].

$$\mathrm{RMS}_i = \sqrt{\frac{\pi f_i S_i}{4\zeta_i}} \tag{17}$$

The relationships between the modal RMS and each of the modal frequency and damping ratio are presented in Figures 14 and 15. In this study, the typhoon-approaching and -leaving phases are referred to as the stages with increasing and decreasing structural responses, respectively. As shown in Figure 14, the natural frequencies decreased as the vibration amplitude increased for all four modes. Interestingly, the frequencies for the two different stages were clearly distinguished at approximately the same vibration level, which was termed "stratification" in previous studies [33]. The natural frequencies were higher during the typhoon-approaching phase, which is consistent with recent observations [14]; however, the underlying mechanism is still being investigated. In terms of the damping ratios (Figure 15), the scatter was significant, and the vibration amplitude did not show a clear pattern, which did not correspond to the amplitude-dependent features observed in the damping ratios of tall buildings under typhoon conditions in previous studies [20,22].

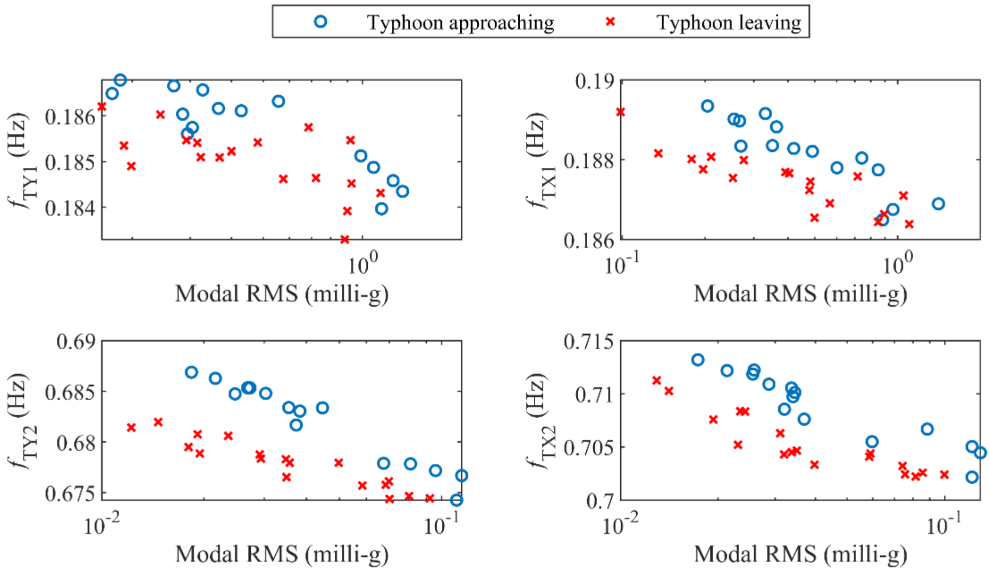

Figure 14. Relationship between modal frequency and modal RMS.

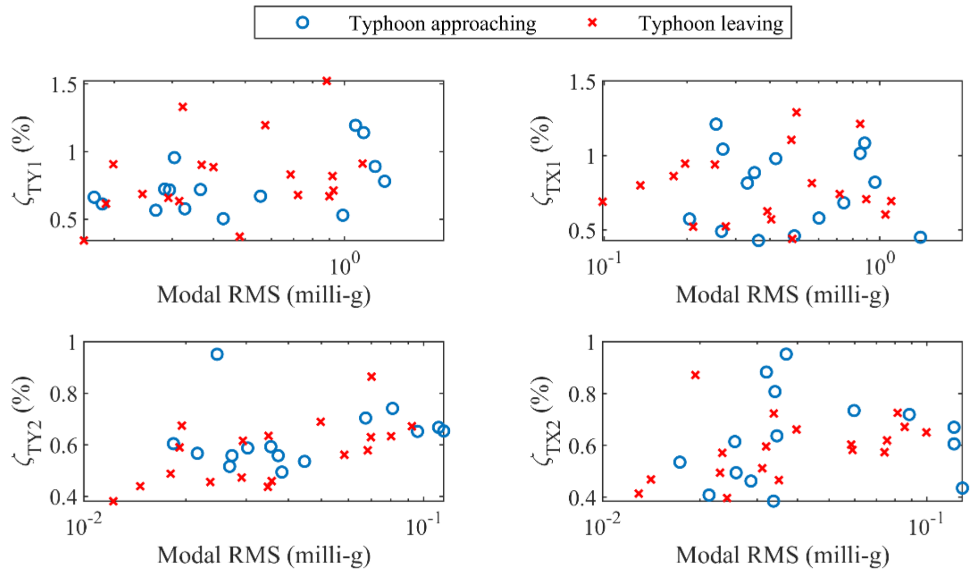

Figure 15. Relationship between damping ratio and modal RMS.

5. Conclusions

Herein, a full-scale measurement of the wind characteristics and wind-induced responses of Leatop Plaza during Typhoon Vicente was presented. The modal properties, i.e., the natural frequency and damping ratio, were identified via the fast Bayesian FFT method and SSI. The identified results and the results predicted by the FEM were compared. On the basis of a detailed analysis of field measurements, the variations in the modal parameters with respect to time and the vibration amplitude were presented and discussed. The main conclusions are as follows:

(1) The turbulence intensity and gust factor decreased as the mean wind speed increased; the average values of the turbulence intensity in the longitudinal and lateral directions were 0.15 and 0.13, respectively. The measured mean longitudinal turbulence intensity was similar to the value specified in the Chinese Building Code.
(2) The von Karman spectrum can describe the energy distribution for fluctuating wind speeds in the lower frequency range at approximately 300 m in height in an urban area.
(3) The identified modal frequencies obtained using the fast Bayesian FFT method agreed well with those identified via SSI, whereas some differences were indicated in terms of the damping ratios. The natural frequencies predicted by the FEM were generally lower than their measured counterparts, with a maximum relative difference of 16.3%.
(4) The natural frequencies of all the modes exhibited an evident time-varying feature, but not for the damping ratios and mode shapes. The largest reductions of the frequencies for the above-mentioned four modes were 1.87%, 1.56%, 1.84%, and 1.55%. Moreover, the natural frequencies exhibited a clear decreasing trend as the vibration amplitude increased, although "stratification" was observed simultaneously. The damping ratios exhibited a large dispersion, and no clear correlation was indicated between the damping ratio and vibration amplitude. The average values of damping ratios for the four modes were 0.79%, 0.78%, 0.60%, and 0.60%.

Author Contributions: Conceptualization, H.P.; methodology, H.P.; formal analysis, H.P.; investigation, H.P.; resources, J.F.; data curation, J.W.; writing—original draft preparation, H.P.; writing—review and editing, H.P., J.W. and J.F.; supervision, J.F.; project administration, J.F.; funding acquisition, H.P. and J.F. All authors have read and agreed to the published version of the manuscript.

Funding: This work was supported by grants from the National Natural Science Foundation of China (grant no. 51925802) and Guangzhou Grants-in-Aid for Science and Technology (202201020176, 202201010550).

Data Availability Statement: Not applicable.

Acknowledgments: The authors would like to thank Siu-Kui Au (Nanyang Technological University, Singapore; ivanau@ntu.edu.sg) for kindly providing the Matlab p-code for the BAYOMA in this work.

Conflicts of Interest: The authors declare no conflict of interest.

References

1. Ohkuma, T.; Marukawa, H.; Niihori, Y.; Kato, N. Full-scale measurement of wind pressures and response accelerations of a high-rise building. *J. Wind. Eng. Ind. Aerodyn.* **1991**, *38*, 185–196. [CrossRef]
2. Hu, J.; Li, Z.; Zhao, Z. Field Measurement on Translational and Torsional Wind-Induced Response of a High-Rise Building during Typhoon Khanun. *Buildings* **2022**, *12*, 1698. [CrossRef]
3. Huang, M.; Xu, Q.; Xu, H.; Ni, Y.Q.; Kwok, K. Probabilistic assessment of vibration exceedance for a full-scale tall building under typhoon conditions. *Struct. Des. Tall Spec. Build.* **2018**, *27*, e1516. [CrossRef]
4. Kijewski-Correa, T.; Kilpatrick, J.; Kareem, A.; Kwon, D.K.; Bashor, R.; Kochly, M.; Young, B.S.; Abdelrazaq, A.; Galsworthy, J.; Isyumov, N.; et al. Validating wind-induced response of tall buildings: Synopsis of the Chicago full-scale monitoring program. *J. Struct. Eng.* **2006**, *132*, 1509–1523. [CrossRef]
5. Fu, J.Y.; Wu, J.R.; Xu, A.; Li, Q.S.; Xiao, Y.Q. Full-scale measurements of wind effects on Guangzhou West Tower. *Eng. Struct.* **2012**, *35*, 120–139. [CrossRef]
6. Li, Q.S.; Han, X.L.; Zhou, K. Effect of time-variant structural modal parameters on accurate estimation of wind-induced dynamic responses of high-rise buildings during typhoons. *J. Build. Eng.* **2022**, *56*, 104783. [CrossRef]
7. Jeary, A.P. Damping in tall buildings—A mechanism and a predictor. *Earthq. Eng. Struct. Dyn.* **1986**, *14*, 733–750. [CrossRef]

8. Jeary, A.P. Establishing non-linear damping characteristics of structures from non-stationary response time-histories. *Struct. Eng.* **1992**, *70*, 61–66.
9. Jeary, A.P. The description and measurement of nonlinear damping in structures. *J. Wind. Eng. Ind. Aerodyn.* **1996**, *59*, 103–114. [CrossRef]
10. Tamura, Y.; Suganuma, S.Y. Evaluation of amplitude-dependent damping and natural frequency of buildings during strong winds. *J. Wind. Eng. Ind. Aerodyn.* **1996**, *59*, 115–130. [CrossRef]
11. Li, Q.S.; Fang, J.Q.; Jeary, A.P.; Wong, C.K. Full scale measurements of wind effects on tall buildings. *J. Wind. Eng. Ind. Aerodyn.* **1998**, *74*, 741–750. [CrossRef]
12. Li, Q.S.; Fu, J.Y.; Xiao, Y.Q.; Li, Z.N.; Ni, Z.H.; Xie, Z.N.; Gu, M. Wind tunnel and full-scale study of wind effects on China's tallest building. *Eng. Struct.* **2006**, *28*, 1745–1758. [CrossRef]
13. Li, Q.S.; Li, X.; Chan, P.W. Impact of a Fifty-Year-Recurrence Super Typhoon on Skyscrapers in Hong Kong: Large-Scale Field Monitoring Study. *J. Struct. Eng.* **2021**, *147*, 04021004. [CrossRef]
14. Pan, H.; Au, S.K.; Fu, J.; Xu, A.; He, Y. Field measurement and wind tunnel experimental investigation of a supertall building with closely spaced modes under typhoon Mangkhut. *J. Wind. Eng. Ind. Aerodyn.* **2022**, *226*, 105033. [CrossRef]
15. Pan, H.; Xie, Z.; Xu, A.; Zhang, L. Wind effects on Shenzhen Zhuoyue Century Center: Field measurement and wind tunnel test. *Struct. Des. Tall Spec. Build.* **2017**, *26*, e1376. [CrossRef]
16. Xie, Z.; Liu, C.; Yu, X. Field measurements and wind tunnel experimental investigations of wind effects on Guangzhou West Tower. *Struct. Des. Tall Spec. Build.* **2020**, *29*, e1774. [CrossRef]
17. Zhou, K.; Li, Q.S. Investigation of time-varying structural dynamic properties of high-rise buildings under typhoon conditions. *J. Build. Eng.* **2022**, *46*, 103796. [CrossRef]
18. Sun, M.; Li, Q. Evaluation of modal properties of high-rise buildings under severe typhoon conditions using correlation function-based modal identification methods. *J. Wind. Eng. Ind. Aerodyn.* **2022**, *229*, 105140. [CrossRef]
19. Zhang, L.; Hu, X.; Xie, Z.; Shi, B.; Zhang, L.; Wang, R. Field measurement study on time-varying characteristics of modal parameters of super high-rise buildings during super typhoon. *J. Wind. Eng. Ind. Aerodyn.* **2020**, *200*, 104139. [CrossRef]
20. Hua, X.G.; Xu, K.; Wang, Y.W.; Wen, Q.; Chen, Z.Q. Wind-induced responses and dynamic characteristics of a super-tall building under a typhoon event. *Smart Struct. Syst.* **2020**, *25*, 81–96.
21. Xu, A.; Xie, Z.; Gu, M.; Wu, J. Amplitude dependency of damping of tall structures by the random decrement technique. *Wind. Struct.* **2015**, *21*, 159–182. [CrossRef]
22. Li, Z.; Fu, J.; He, Y.; Liu, Z.; Wu, J.; Rao, R.; Ng, C.T. Structural responses of a supertall building subjected to a severe typhoon at landfall. *Appl. Sci.* **2020**, *10*, 2965. [CrossRef]
23. *GB 50009-2012*; Load Code for the Design of Building Structures. China Building Industry Press: Beijing, China, 2012.
24. Cao, S.; Tamura, Y.; Kikuchi, N.; Saito, M.; Nakayama, I.; Matsuzaki, Y. Wind characteristics of a strong typhoon. *J. Wind. Eng. Ind. Aerodyn.* **2009**, *97*, 11–21. [CrossRef]
25. Wang, Y.W.; Ni, Y.Q. Full-scale monitoring of wind effects on a supertall structure during six tropical cyclones. *J. Build. Eng.* **2022**, *45*, 103507. [CrossRef]
26. Katafygiotis, L.S.; Yuen, K.V. Bayesian spectral density approach for modal updating using ambient data. *Earthq. Eng. Struct. Dyn.* **2001**, *30*, 1103–1123. [CrossRef]
27. Yuen, K.V.; Katafygiotis, L.S. Bayesian time–domain approach for modal updating using ambient data. *Probabilistic Eng. Mech.* **2001**, *16*, 219–231. [CrossRef]
28. Yuen, K.V.; Katafygiotis, L.S. Bayesian fast Fourier transform approach for modal updating using ambient data. *Adv. Struct. Eng.* **2003**, *6*, 81–95. [CrossRef]
29. Au, S.K. *Operational Modal Analysis*; Springer Nature: Singapore, 2017.
30. Au, S.K.; Zhang, F.L.; To, P. Field observations on modal properties of two tall buildings under strong wind. *J. Wind. Eng. Ind. Aerodyn.* **2012**, *101*, 12–23. [CrossRef]
31. Peeters, B.; De Roeck, G. Reference-based stochastic subspace identification for output-only modal analysis. *Mech. Syst. Signal Process.* **1999**, *13*, 855–878. [CrossRef]
32. He, Y.C.; Li, Z.; Fu, J.Y.; Wu, J.R.; Ng, C.T. Enhancing the performance of stochastic subspace identification method via energy-oriented categorization of modal components. *Eng. Struct.* **2021**, *233*, 111917. [CrossRef]
33. Liu, C.; Xie, Z.; Zhang, L.; Shi, B.; Fu, J.; Deng, T. Field measurements of wind effects on a super high-rise building during typhoons. *Wind. Struct.* **2021**, *33*, 383–395.